– Electronic Supporting Information –

Iodine Passivation Facilitates On-Surface Synthesis of Robust Regular Conjugated Two-Dimensional Organogold Networks on Au(111)

Arash Badami-Behjat[1], Gianluca Galeotti[1], Rico Gutzler[1], Dominik L. Pastoetter[2],

Wolfgang M. Heckl[1], Xinliang Feng[2,3], and Markus Lackinger[1,*]

[1] Deutsches Museum, Museumsinsel 1, 80538 Munich, Germany and Department of Physics, Technische Universität München, James-Franck-Str. 1, 85748 Garching, Germany;

[2] Center for Advancing Electronics Dresden & Faculty of Chemistry and Food Chemistry, Technische Universität Dresden, 01069 Dresden, Germany;

[3] Max Planck Institute of Microstructure Physics, Weinberg 2, 06120 Halle, Germany;

Materials and Methods

-Sample preparation

Au(111) single crystal substrates were prepared by the usual cycles of Ar^+-ion-sputtering (850 eV, 1×10^{-5} mbar, 10 min) and annealing (490 °C, 15 min), and their cleanliness was verified by STM imaging.

Iodine passivation was achieved by exposing freshly prepared Au(111) to I_2 vapor in a separate preparation chamber to avoid contamination of the main chamber. The reactive I-Au(111) surfaces (cf. ESI Figure S1 and Figure 2 of the main manuscript) were prepared by exposing the sample to 5×10^{-7} mbar of I_2 for 10 min. To desorb excess iodine and for equilibration, the samples were then annealed in UHV in the main chamber at 180 °C (30 min ramp time and 15 min dwell time). This procedure results in a surface where the iodine layer still has areas that are not densely packed (see Figures S1 and S4). In contrast, fully closed, densely packed iodine monolayers were obtained by a 20-fold increased iodine exposure, i.e. 5×10^{-6} mbar I_2 for 20 min followed by annealing at 190 °C for 15 min. These samples were found to be unreactive for debromination (see Figure S2).

The 2,5,9,12-tetrabromoanthra[1,2-b:4,3-b':5,6-b'':8,7-b''']tetrathiophene (TBATT) precursor molecules were synthesized according to a procedure reported by Perepichka et al.[1] Before deposition from a home-built Knudsen cell,[2] TBATT was thoroughly outgassed at 300 °C for an extended period of time. Deposition was performed with a crucible temperature of 290 °C. To account for the different sticking coefficients of bare and iodine-passivated Au(111), different deposition times were used, that is 3 - 4 min for bare Au(111) and 10 min for I-Au(111).

-STM and STS experiments

A home-built low-temperature STM controlled by a Nanonis BP 4 electronics was used, operating in Ultra-High Vacuum (UHV) at a base pressure of 1×10^{-10} mbar. Unless otherwise noted, the STM experiments were performed at low temperatures. The instrument is cooled by a flow cryostat with liquid nitrogen, resulting in sample temperatures of ~80 K. Electrochemically etched tungsten tips were used and in-situ conditioned by Ar^+-ion sputtering with an applied counter voltage.[3] The bias voltage was applied to the STM tip, but stated bias polarities refer to the sample. The WSxM software was used for image processing comprised of plane correction and line-by-line levelling.[4]

STS experiments were also performed at low temperature after an extended stabilization period of typically >24 h. The dI/dV spectra were acquired with the Lock-In technique using a modulation frequency of 329 Hz and a modulation amplitude of 30 mV with a voltage slew rate of 100 V s^{-1}, a setting time of 300 ms and an integration time of 300 ms for each data point.

-DFT calculations

Orca 4.2.0[5] was used for DFT calculations of organogold aggregates (cf. Figure S9) with the B3LYP functional[6] and the def2-SVP basis set.[7]

The Quantum Espresso 6.5[8] code was used for band structure calculations of the periodic organogold networks, employing a plane-wave basis set, the Perdew-Burke-Ernzerhof (PBE) functional,[9] and norm-conserving Martins-Troullier pseudopotentials.[10] A kinetic energy cutoff of 60 Ry and a charge density cutoff of 240 Ry were used. An additional SCF step was performed on the optimized structure with a finer k-point mesh of $8\times8\times1$ points prior to the band structure calculation. The vacuum along the z-direction perpendicular to the structure was >10 Å in order to suppress interaction between layers.

Additional STM data

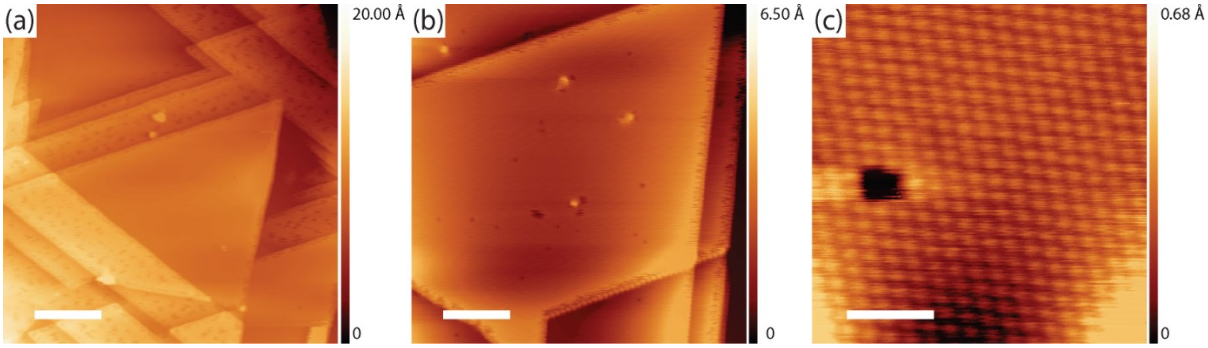

Figure S1 STM images of a still reactive iodine passivation layer on Au(111) prepared by mild iodine exposure (5×10^{-7} mbar of I_2 for 10 min) acquired at low temperature. **(a) / (b)** Overview and **(c)** close-up showing a small iodine vacancy island. These STM images reflect the stage of the I-Au(111) samples before they were annealed to form the networks. They confirm that the iodine monolayer is not fully closed prior to the thermal treatment to form the networks but exhibits a fair amount of vacancy islands. As shown in (b), the passivation of Au(111) is incomplete, especially at the substrate step-edges. (tunneling parameters and scale bars: (a) +1.0 V, 100 pA, 20 nm; (b) +1.0 V, 100 pA, 10 nm; (c) +1.0 V, 100 pA, 2 nm, all STM images were acquired at low temperature)

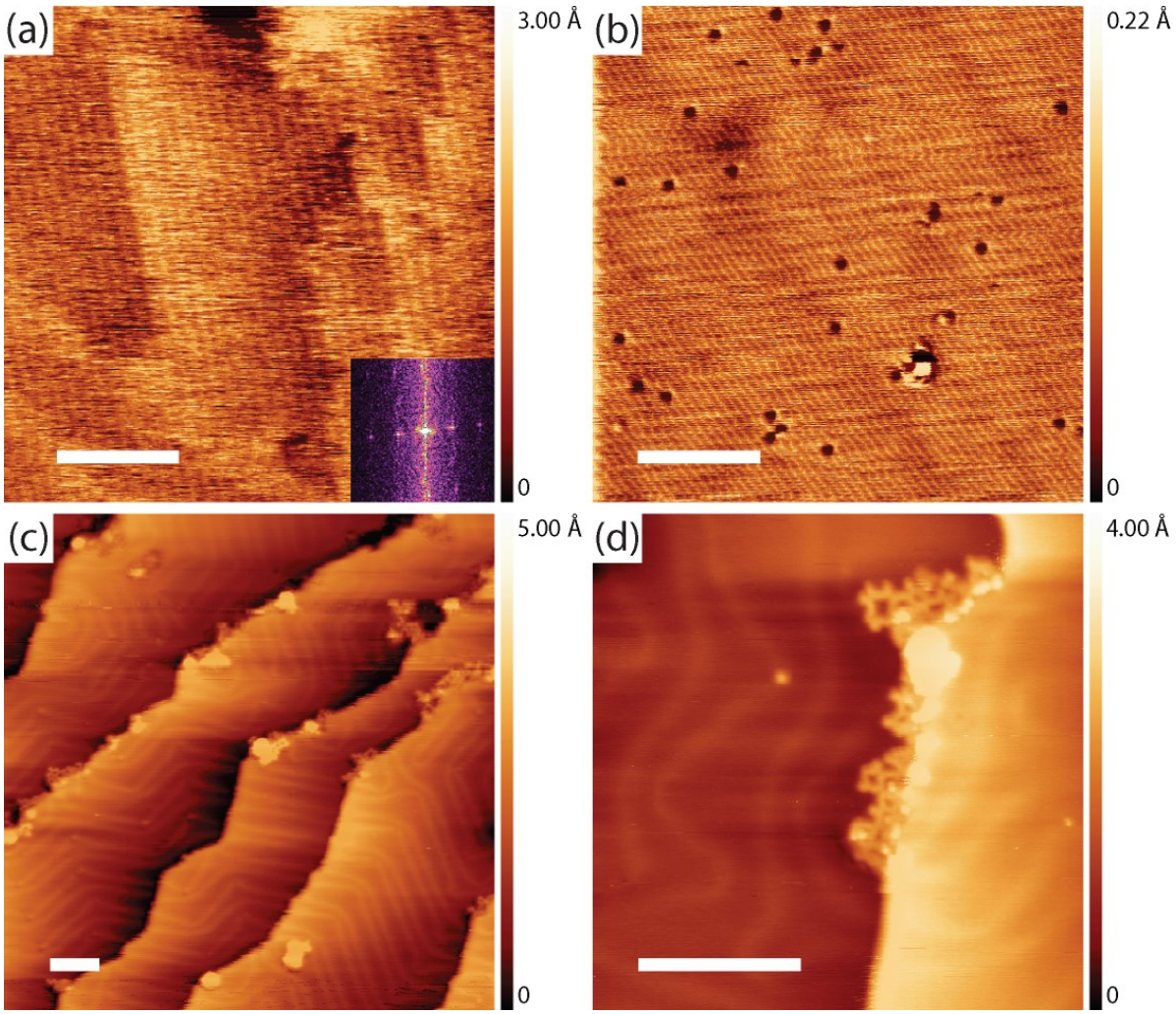

Figure S2 STM images of TBATT molecules deposited on a highly (5×10^{-6} mbar I_2 for 20 min) iodinated Au(111) sample acquired **(a)** directly after deposition, **(b)** after annealing this sample at 250 °C for 15 min and **(c)** / **(d)** after further annealing at 350 °C for 15 min. The stripes in (a) have a spacing of 1.2 ± 0.1 nm as derived from the 2D Fast-Fourier-Transform (shown as inset in (a)), which is in agreement with the lattice parameter of the self-assembled structure (cf. main manuscript). We conclude that these stripes correspond to a self-assembly of intact TBATT molecules as expected. In contrast, after annealing at 250 °C, stripes were again observed, but with a significantly smaller stripe spacing of 0.6 ± 0.2 nm. This spacing is consistent with the densely packed iodine monolayer, indicating the desorption of most of the TBATT molecules and also the onset of iodine desorption, resulting in the clearly visible black holes. Upon heating to a higher temperature of 350 °C, the STM images in (c) and (d) show the reappearance of the Au(111) herringbone reconstruction, indicating the desorption of the iodine passivation layer. Smaller patches of molecular networks are observed, but only at the step-edges. We hypothesize that these form when the Au(111) surface becomes accessible by iodine desorption. However, the relatively low coverage suggests that most of the TBATT precursor molecules have already desorbed. (tunneling parameters: (a) +1.1 V, 120 pA; (b) +600 mV, 110 pA; (c) +600 mV, 110 pA; (d) +600 mV, 110 pA; all scale bars are 10 nm, all STM images were acquired at room temperature)

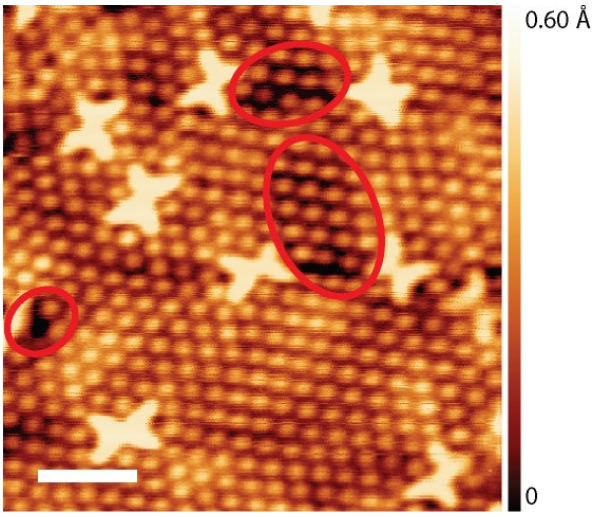

Figure S3 Low temperature STM image of a reactive iodine monolayer prepared with the lower iodine exposure. The image was acquired at low temperature after deposition of the TBATT molecules, but before the networks were formed by sample annealing. The bright butterfly-shaped features correspond to individual unreacted TBATT molecules. Although the iodine monolayer appears densely packed and completely closed at room temperature (see Figure 2 of the main manuscript), low temperature imaging reveals areas where the iodine layer is not densely packed (an example is highlighted by the larger oval). In addition, iodine vacancies can be observed (an example is highlighted by the smaller oval). In contrast, completely densely packed iodine monolayers prepared by a 20-fold increased iodine exposure are no longer reactive (see Figure S2). We conclude that the less densely packed regions are the active sites for the initial debromination and also provide the Au-atoms for the formation of the organogold networks. (tunneling parameters and scale bar: +900 mV, 120 pA, 2 nm, STM image acquired at low temperatures)

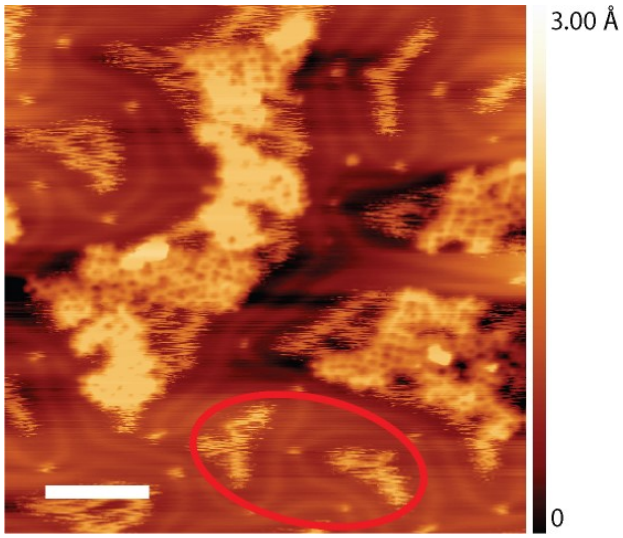

Figure S4 STM images of TBATT-derived organogold networks prepared on a reactive I-Au(111) surface obtained after additional annealing at 300 °C. This image was acquired at room temperature. While the organogold networks could be imaged, the image additionally shows fuzzy appearing features (an example is highlighted by the oval) corresponding to remnants of the mostly desorbed iodine layer. These features disappear completely when the sample is heated to a slightly higher temperature of 320 °C (see Figure 3 of the main manuscript). The characteristic soliton lines of the reappearing Au(111) herringbone reconstruction can also be seen. (tunneling parameters and scale bar: +1.2 V, 120 pA, 10 nm, STM image acquired at low temperature)

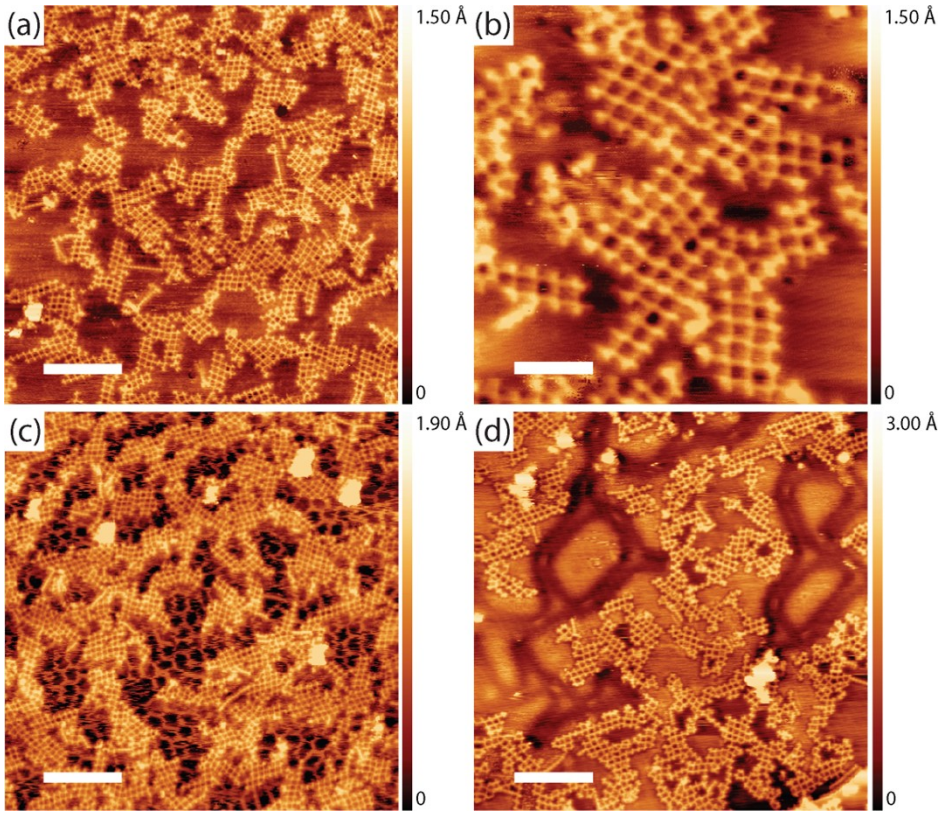

Figure S5 STM images of organogold networks synthesized by co-deposition of TBATT and iodine on bare Au(111). After deposition of the molecules, the samples were exposed to 1×10^{-7} mbar I_2 for **(a)** / **(b)** / **(c)** 10 min and **(d)** 1 min and annealed at 200 °C for 15 min to form the networks. At low temperature, the iodine is immobilized in a filamentous structure, which is not visible at room temperature, but gives a more realistic impression of the iodine coverage. The presence of iodine on the surface mediates the formation of organogold networks that are more regular than those obtained on bare Au(111), but still exhibit more defects than those obtained on I-Au(111) by inducing reversibility in the carbon-Au-carbon bonds. (tunneling parameters and scale bars: (a) +1.3 V, 120 pA, 20 nm; (b) +1.3 V, 120 pA, 6 nm; (c) +1.2V, 120 pA, 20 nm; (d) +1.0 V, 120 pA, 20 nm, STM images (a) / (b) / (d) were acquired at room temperature, and only image (c) was recorded at low temperature.)

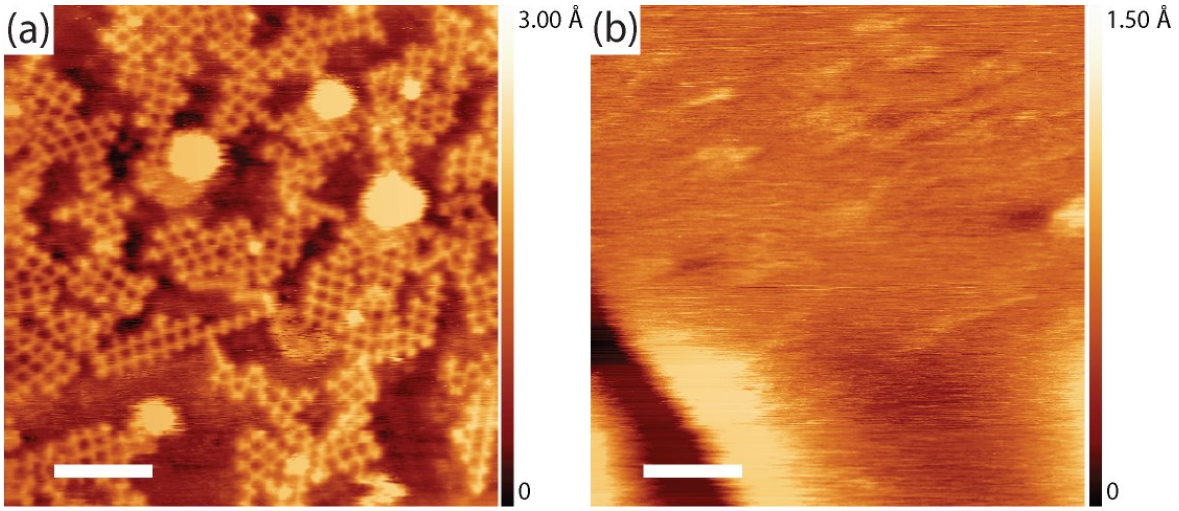

Figure S6 Annealing of organogold networks under reversible conditions in an iodine atmosphere. **(a)** STM image of the organogold networks prepared on I-Au(111) according to the established protocol. **(b)** STM image of the same sample acquired after annealing at 320 °C (30 min ramp time and 15 min dwell time) in a background pressure of 10^{-7} mbar iodine. The sample appears empty, from which we conclude that the networks have desorbed. This was not the case with vacuum annealing (cf. Figure 3 of the main manuscript) and can therefore be attributed to the presence of iodine. It weakens the organometallic carbon-Au-carbon bonds to such an extent that the networks eventually disintegrate and the individual monomers desorb at the high temperature. (tunneling parameters and scale bars: (a) +1.0 V, 120 pA, 10 nm; (b) +1.0 V, 120 pA, 10 nm; both images were acquired at room temperature)

Additional DFT results

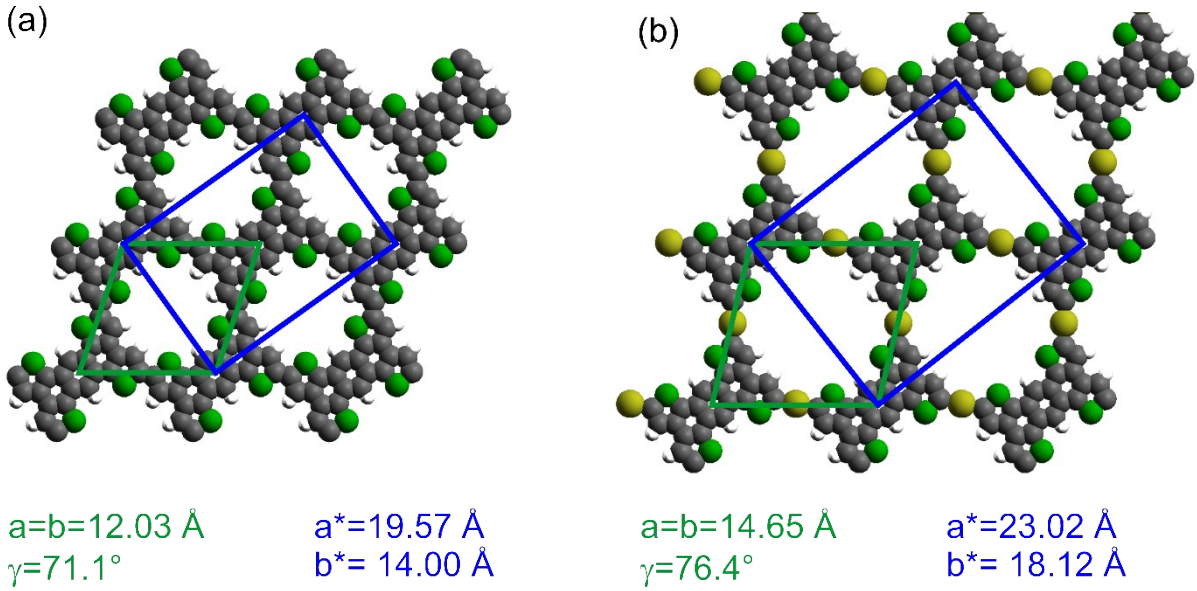

Figure S7 Structures and lattice parameters of DFT-calculated free-standing periodic monolayers (C: grey; H: white; S: green; Au: yellow). **(a)** covalent and **(b)** organogold networks, in which the anthra-tetrathiophene repeat units are linked by either (a) direct carbon-carbon or (b) organometallic carbon-Au-carbon bonds, respectively. Calculations were performed for the primitive unit cell (green rhombus) with optimized parameters indicated on the lower left (also in green). In this case, the lattice parameter directly represents the center-to-center distance between bonded monomers, which is 2.6 Å shorter in the covalent network. This difference can be unambiguously measured within the experimental error of the STM experiment (0.05 nm - 0.10 nm). Thereby the intermolecular carbon-carbon bond measures 1.44 Å, while the bond length of the carbon-Au-carbon bond is 4.03 Å. Crystallographically, the structures are described by a centered rectangular unit cell (blue rectangle) with the lattice parameters (also in blue, marked with asterisks) shown on the lower right.

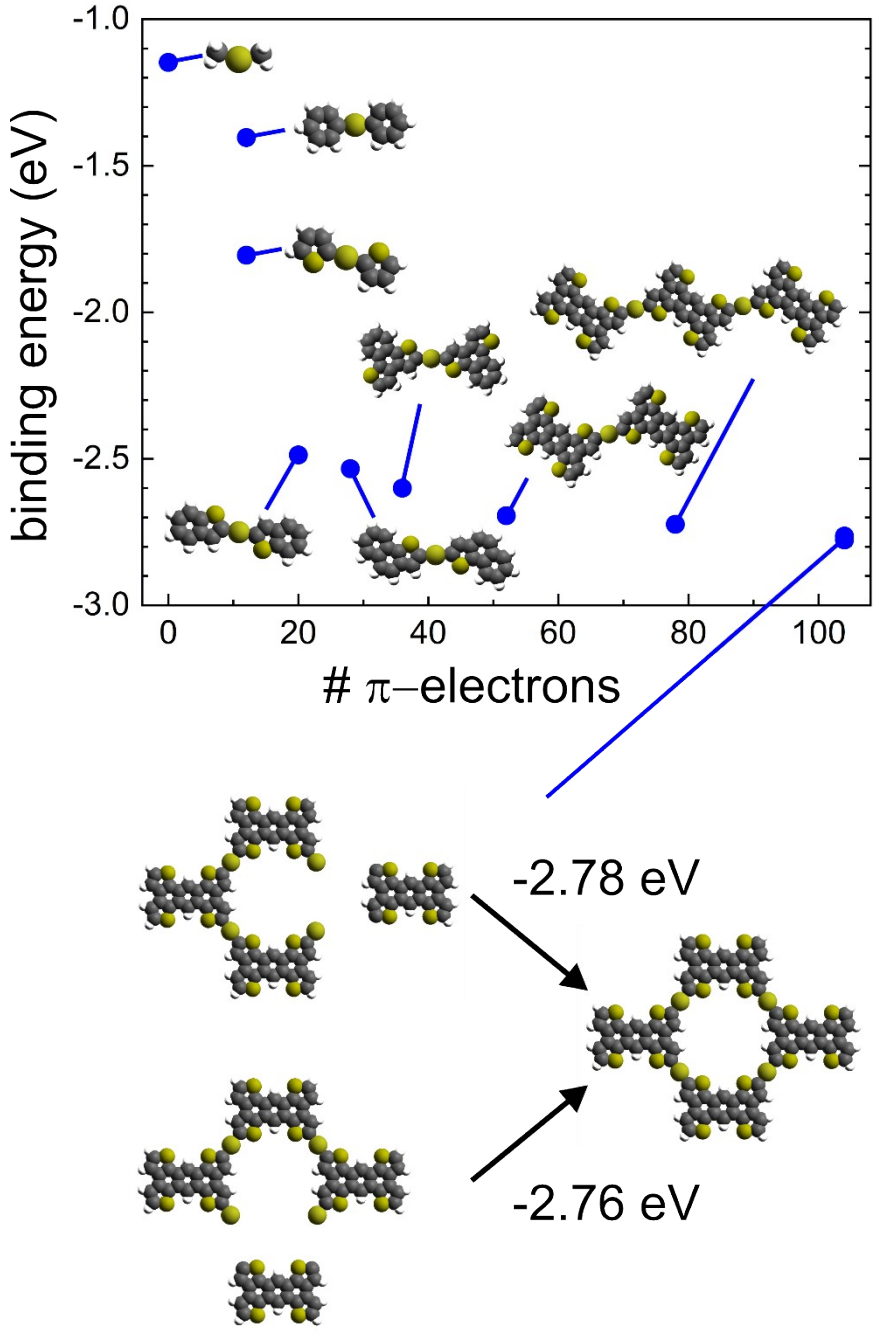

Figure S8 DFT calculations of the binding energies (BE) of carbon-Au-carbon bonds as a function of the size of the organogold aggregates, here represented by the number of π electrons. The corresponding bonded structures are shown for all data points, and the BE values given refer to the formation of a single covalent bond between an organometallic Au-atom and a carbon-centered radical: R-C-Au + ·C-R → R-C-Au-C-R. While the BE of the smallest calculated aggregate (methyl-Au-methyl) is only -1.15 eV, it increases sharply with increasing size of the aromatic system and plateaus at -2.69 eV for 52 π electrons, corresponding to the organogold anthra-tetrathiophene dimer. In the largest calculated aggregate, the 2×2 anthra-tetrathiophene tetramer, the BE increases moderately to -2.76 eV / -2.78 eV. For the 2×2 tetramer, there are two non-equivalent binding pathways, as shown below, that, however, result in nearly similar BE. Notably, although the thiophene-Au-thiophene and the phenyl-Au-phenyl dimers both have 12 π electrons, the thiophene has a significantly larger BE of -1.81 eV compared to -1.41 for the phenyl. This highlights the bond-strengthening influence of sulfur-containing heterocycles on organogold structures. In summary, the large BE for the aromatic thiophene-containing organogold aggregates reflects the experimentally found high thermal stability.

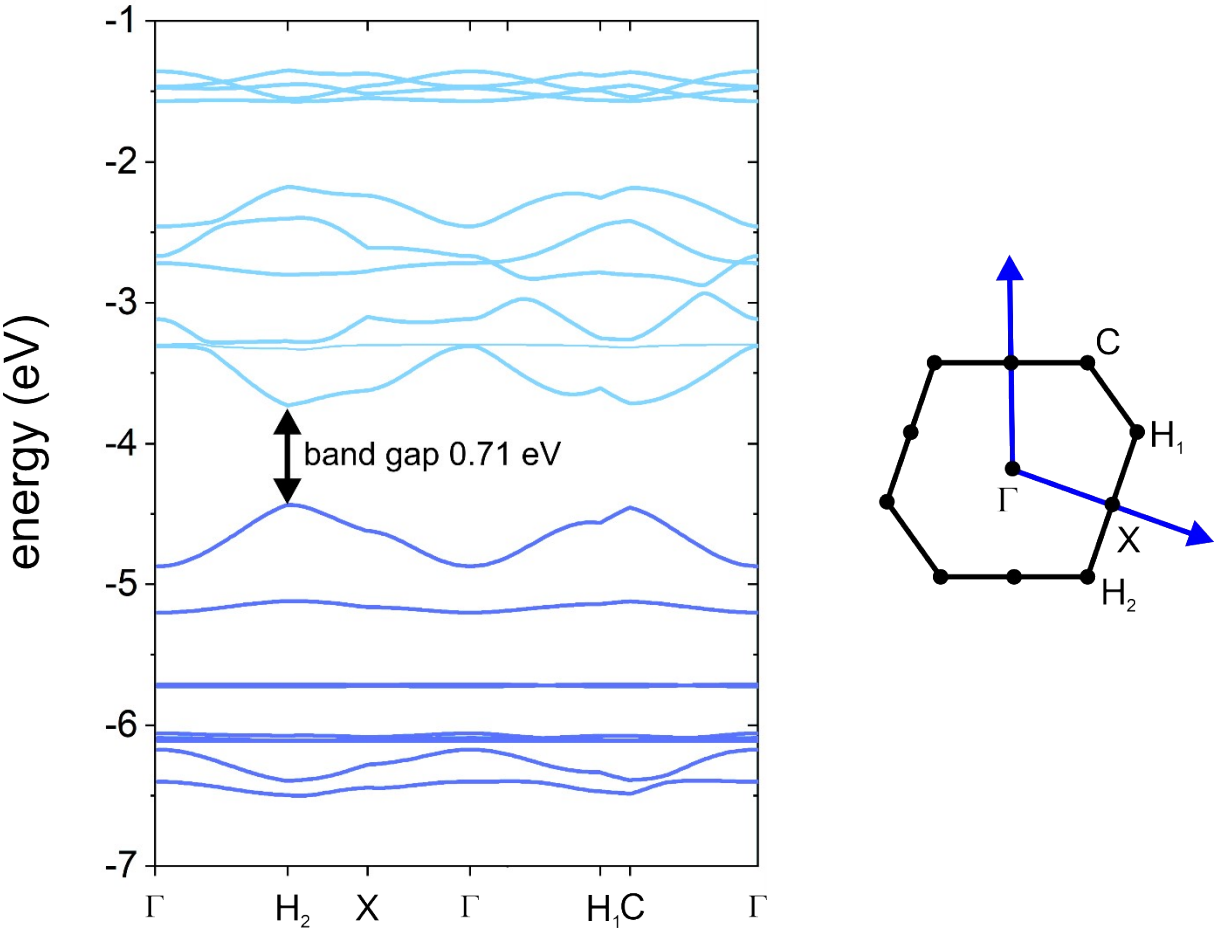

Figure S9 DFT calculated electronic band structure of the organogold network shown for the primitive unit cell (see Figure S7b). The corresponding first Brillouin zone is shown on the right hand side. The calculated electronic band gap as indicated amounts to 0.71 eV. The obvious dispersion of the bands indicates π-electron conjugation through the carbon-Au-carbon linkages as also indicated by the spatial distribution of frontier molecular orbitals (cf. Figure S10).

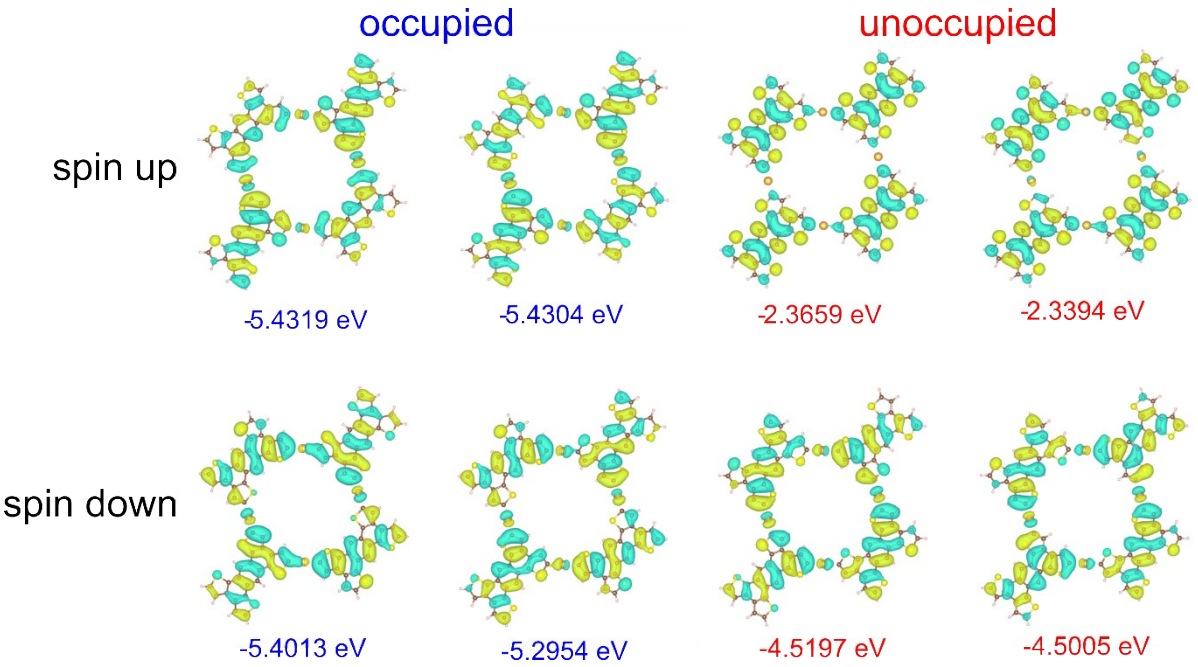

Figure S10 DFT-calculated spatial distribution of the frontier molecular orbitals of the 2×2 organogold tetramer (structure shown in the background). Orbitals for spin up (down) are depicted in the upper (lower) row. The two columns on the left (right) depict occupied (unoccupied) molecular orbitals. Respective energies are indicated below in blue (red) for the occupied (unoccupied) molecular orbitals. These orbitals indicate conjugation through the carbon-Au-carbon bonds.

References

(1) Brusso, J. L.; Hirst, O. D.; Dadvand, A.; Ganesan, S.; Cicoira, F.; Robertson, C. M.; Oakley, R. T.; Rosei, F.; Perepichkat, D. F. Two-Dimensional Structural Motif in Thienoacene Semiconductors: Synthesis, Structure, and Properties of Tetrathienoanthracene Isomers. *Chem. Mater.* **2008**, *20*, 2484-2494.
(2) Gutzler, R.; Heckl, W. M.; Lackinger, M. Combination of a Knudsen Effusion Cell with a Quartz Crystal Microbalance: In-Situ Measurement of Molecular Evaporation Rates with a Fully Functional Deposition Source. *Rev. Sci. Instrum.* **2009**, *81*, 015108.
(3) Schmucker, S. W.; Kumar, N.; Abelson, J. R.; Daly, S. R.; Girolami, G. S.; Bischof, M. R.; Jaeger, D. L.; Reidy, R. F.; Gorman, B. P.; Alexander, J.; Ballard, J. B.; Randall, J. N.; Lyding, J. W. Field-Directed Sputter Sharpening for Tailored Probe Materials and Atomic-Scale Lithography. *Nat. Commun.* **2012**, *3*.
(4) Horcas, I.; Fernandez, R.; Gomez-Rodriguez, J. M.; Colchero, J.; Gomez-Herrero, J.; Baro, A. M. Wsxm: A Software for Scanning Probe Microscopy and a Tool for Nanotechnology. *Rev. Sci. Instrum.* **2007**, *78*, 013705.
(5) Neese, F. The Orca Program System. *Wires. Comput. Mol. Sci.* **2012**, *2*, 73-78.
(6) Stephens, P. J.; Devlin, F. J.; Ashvar, C. S.; Chabalowski, C. F.; Frisch, M. J. Theoretical Calculation of Vibrational Circular-Dichroism Spectra. *Faraday Discuss.* **1994**, *99*, 103-119.
(7) Weigend, F.; Ahlrichs, R. Balanced Basis Sets of Split Valence, Triple Zeta Valence and Quadruple Zeta Valence Quality for H to Rn: Design and Assessment of Accuracy. *Phys. Chem. Chem. Phys.* **2005**, *7*, 3297-3305.
(8) Giannozzi, P.; Baroni, S.; Bonini, N.; Calandra, M.; Car, R.; Cavazzoni, C.; Ceresoli, D.; Chiarotti, G. L.; Cococcioni, M.; Dabo, I.; Dal Corso, A.; de Gironcoli, S.; Fabris, S.; Fratesi, G.; Gebauer, R.; Gerstmann, U.; Gougoussis, C.; Kokalj, A.; Lazzeri, M.; Martin-Samos, L.; et al. Quantum Espresso: A Modular and Open-Source Software Project for Quantum Simulations of Materials. *J. Phys.-Condens. Mat.* **2009**, *21*.
(9) Perdew, J. P.; Burke, K.; Ernzerhof, M. Generalized Gradient Approximation Made Simple. *Phys. Rev. Lett.* **1996**, *77*, 3865-3868.
(10) Troullier, N.; Martins, J. L. Efficient Pseudopotentials for Plane-Wave Calculations. *Phys. Rev. B* **1991**, *43*, 1993-2006.